

DO-TH 04/07
hep-ph/
September 2004.

Electron Spectra in the Ionization of Atoms by Neutrinos

G.J. Gounaris^a, E.A. Paschos^b, and P.I. Porfyriadis^a

^a*Department of Theoretical Physics, Aristotle University of Thessaloniki
GR-54006 Thessaloniki, Greece*

^b*Universität Dortmund, Institut für Physik,
D-44221 Dortmund, Germany*

Abstract

For neutrinos of $\mathcal{O}(10\text{keV})$ energies, their oscillation lengths are less than a few hundred meters, thereby suggesting the fascinating idea of oscillation experiments of small geometrical size. To help evaluating this idea, we calculate the ionization cross sections of H, He, Ne, and Xe, using any neutrino flavor, in the few keV energy range. We find that the atomic ionizations cross sections per electron, are always smaller than the neutrino cross section off free electrons, approaching it from below as the energy increases to the 100 keV region. At the 10-20 keV range though, atomic binding effects are very important, particularly for the heavier atoms, inducing an almost a factor of two reduction for the Xe ionization cross section compared to the free electron case.

PACS numbers:13.15.+g

1 Introduction

Neutrino interactions have been observed and analyzed at energies from a few MeV (in reactor and solar neutrino experiments) [1], to several hundred GeV at accelerators. The lower keV energy range though, has not attracted much interest up to now, due to the smaller cross sections there.

Nevertheless, when intense neutrino fluxes from radioactive decays become available, the possibility of very interesting experiments may arise, such as the testing of the solar neutrino oscillations using terrestrial experiments of rather small geometrical size [2]. To see this, we remark that recent results from the KamLAND experiment gives [3]

$$\Delta m_{12}^2 = 8.2_{-0.3}^{+0.3} \times 10^{-5} \text{ eV}^2, \quad \tan^2 \theta_{12} = 0.39_{-0.07}^{+0.09}, \quad (1)$$

which would suggest a corresponding neutrino oscillation length of about 15 meters for 1 keV neutrinos, increasing to 150 meters when the energy reaches the 10 keV level. The oscillation length associated to $\Delta m_{13}^2 \simeq \Delta m_{23}^2$ is about 27 times smaller [4].

To perform oscillation measurements at keV energies, the ionization of atoms by neutrinos may be used, taking of course into account the binding of the electrons. As an example we mention that the realization of an intense Tritium source may allow the study of $\bar{\nu}_e$ oscillations in a room size experiment.

Such experiments may also help in investigating the weak interaction couplings at very low energies like *e.g.* the search for measurable contributions from an anomalous neutrino magnetic moment [2]. These are interesting questions, which were never investigated at very low energies, and may provide useful additional information on neutrino physics.

On the theoretical side, there are three calculations known to us investigating such effects. Some time ago [5], we computed the total cross section on free and bound electrons where atomic effects on the bound electron were evident. At that time we studied the three atoms H, He and Ne where the binding effects were present but not very large. The result was that the ionization cross section per electron is smaller than the cross section from free electrons [5], and never larger [6]. Moreover, this ionization cross section always decreases as we proceed from H to He to Ne, obviously due to the increase of the binding [5].

Another article [7] computed the energy spectrum of electrons knocked out from $^{19}F(Z = 9)$ and $^{96}Mo(Z = 42)$ atoms. The authors found that these spectra differ significantly from the free scattering case.

For planning and carrying out the new experiments mentioned above, it is useful to have the energy-spectra of the ionization electrons for the noble gases He, Ne, Ar, Kr, Xe, with kinetic energies higher than about 10 eV [2]. The aim of the present paper is to calculate such spectra.

At the very low energies we are interested in, the Standard Model dynamics described by the diagrams in Fig.1 induce the effective interaction Lagrangian

$$L_{e\nu} = -\frac{G_F}{\sqrt{2}} \left\{ \left[\bar{\nu}_e \gamma^\rho \frac{(1 - \gamma_5)}{2} \nu_e \right] \left[v_e \bar{e} \gamma_\rho e - a_e \bar{e} \gamma_\rho \gamma_5 e \right] \right.$$

$$+ \left[\bar{\nu}_\mu \gamma^\rho \frac{(1 - \gamma_5)}{2} \nu_\mu + \bar{\nu}_\tau \gamma^\rho \frac{(1 - \gamma_5)}{2} \nu_\tau \right] \left[\tilde{v}_e \bar{e} \gamma_\rho e - \tilde{a}_e \bar{e} \gamma_\rho \gamma_5 e \right] \right\} , \quad (2)$$

describing the electron interactions with any neutrino flavor. The ν_e and (ν_μ, ν_τ) couplings are respectively given by

$$\begin{aligned} v_e &= 1 + 4s_W^2 & a_e &= 1 & , \\ \tilde{v}_e &= -1 + 4s_W^2 & \tilde{a}_e &= -1 & , \end{aligned} \quad (3)$$

while G_F is the usual Fermi coupling.

We first concentrate on the $\nu_e(\bar{\nu}_e)$ cases. From (2), the squared invariant amplitude $|F|^2$, summed over all initial and final electron spin-states for the process

$$\nu_e(P_1) e^-(P_2) \rightarrow \nu_e(P_3) e^-(P_4) \quad (4)$$

is calculated, with the four-momenta being indicated in parentheses. The various particle energies are denoted below by E_j , and the standard variables

$$s = (P_1 + P_2)^2 > m_e^2 \quad , \quad t = (P_1 - P_3)^2 \quad , \quad u = (P_1 - P_4)^2 \quad , \quad (5)$$

are used. We note that (4) describes the ν_e scattering from either a free or bound electron, the difference being determined by E_2 ; and, of course, the folded in momentum-wave function in the bound electron case.

We start from the case where the initial electron is free, so that $P_1^2 = P_3^2 = 0$, $P_2^2 = P_4^2 = m_e^2$, with m_e being the electron mass. Summing over all initial and final electron spin states, we then have

$$\begin{aligned} |F(\nu_e e^- \rightarrow \nu_e e^-)|_{\text{free}}^2 &= 2G_F^2 \left\{ (v_e + a_e)^2 (s - m_e^2)^2 \right. \\ &\quad \left. + (v_e - a_e)^2 (u - m_e^2)^2 + 2m_e^2 (v_e^2 - a_e^2) t \right\} . \end{aligned} \quad (6)$$

Due to crossing, the corresponding $|F|^2$ expression for the $\bar{\nu}_e$ case is simply obtained from the ν_e result, by interchanging $s \leftrightarrow u$ in (6).

In the lab system where the initial electron is at rest ($E_2 = m_e$), the differential cross section describing the energy distribution of the final electron is

$$\begin{aligned} \frac{d\sigma(\nu_e e^- \rightarrow \nu_e e^-)}{dE_4} \Big|_{\text{free}} &= \frac{m_e G_F^2}{8\pi E_1^2} \left\{ (v_e + a_e)^2 E_1^2 + (v_e - a_e)^2 (E_1 + m_e - E_4)^2 \right. \\ &\quad \left. + m_e (v_e^2 - a_e^2) (m_e - E_4) \right\} . \end{aligned} \quad (7)$$

Integrating (7) over the allowed range

$$m_e \leq E_4 \leq m_e + \frac{2E_1^2}{m_e + 2E_1} , \quad (8)$$

we then obtain

$$\begin{aligned}\sigma_{\text{free}}^{\nu e} &\equiv \sigma(\nu_e e^- \rightarrow \nu_e e^-) \Big|_{\text{free}} = \frac{m_e G_F^2 E_1}{8\pi} \left\{ (v_e + a_e)^2 \frac{2E_1}{m_e + 2E_1} \right. \\ &+ \left. \frac{1}{3} (v_e - a_e)^2 \left[1 - \frac{m_e^3}{(m_e + 2E_1)^3} \right] - (v_e^2 - a_e^2) \frac{2m_e E_1}{(m_e + 2E_1)^2} \right\} ,\end{aligned}\quad (9)$$

for the ν_e total cross section off free electrons.

Starting from (7), we present in¹ Fig.2 the energy distribution of the final electrons, in ν_e and $\bar{\nu}_e$ scattering off free initial e^- . In these figures $E_e \equiv E_4$ is the final electron energy, and E_ν ($E_{\bar{\nu}}$) denote the incoming neutrino (antineutrino) energy E_1 . As seen there, the energy distribution always has maximum at small E_e , which is also seen in all $\nu_e(\bar{\nu}_e)$ -induced ionization cases; see below.

In Section 2 the formalism describing the ionization of atoms though neutrino (antineutrino) scattering is presented. This is done first for the Hydrogen atom, and it is subsequently generalized to any atom characterized by complete electronic shells.

In Section 3, we present the results for the energy distributions of the knocked out ionization electron in $\nu_e(\bar{\nu}_e)$ scattering for H, as well as for He, Ne and Xe, using the analytic non-relativistic Roothann-Hartree-Fock wave functions published in [8]. In addition, we also present results for Xe ionization through ν_μ or ν_τ scattering, which might be generated through ν_e oscillation. Results for the integrated cross sections are also given in the same Section 3. The conclusions are presented in Section 4, while important details on the kinematics and atomic wave functions are relegated to the Appendices A.1 and A.2 respectively.

2 The formalism.

The ionization of atoms through neutrino scattering off atomic electrons, requires from atomic physics the electron binding energy and the wave functions in momentum space. The energy of the initial bound electron is fixed by the binding energy ϵ , so that

$$E_2 = m_e + \epsilon , \quad (10)$$

with ϵ being negative. For the simplest H atom, ϵ is fixed by the Balmer formula, while for more complicated atoms, we use the experimental measurements [9].

The three-dimensional momentum of the bound electron however, (compare definitions in (A.1)), varies according to the probability distribution

$$|\tilde{\Psi}_{nlm}(p_2, \theta_2, \phi_2)|^2 \frac{p_2^2 dp_2 d \cos \theta_2 d \phi_2}{(2\pi)^3} , \quad (11)$$

¹We always use $s_W^2 = 0.2312$.

determined by the momentum wave function² $\tilde{\Psi}_{nlm}(p_2, \theta_2, \phi_2)$, when electron spin effects are neglected. Therefore, the bound electron may get off-shell with an effective squared-mass given by

$$\tilde{m}^2 \equiv P_2^2 = E_2^2 - p_2^2 , \quad (12)$$

so that, the standard kinematical variables defined in (5) satisfy

$$s + t + u = \tilde{m}^2 + m_e^2 . \quad (13)$$

The squared invariant amplitude for the ν_e -electron subprocess, summed over all initial and final electron spin states³, is written as [5]

$$\begin{aligned} |F(\nu_e e^- \rightarrow \nu_e e^-)|^2 &= 2G_F^2 \left\{ (v_e + a_e)^2 (s - m_e^2)(s - \tilde{m}^2) \right. \\ &\quad \left. + (v_e - a_e)^2 (u - m_e^2)(u - \tilde{m}^2) + 2m_e^2(v_e^2 - a_e^2)t \right\} , \end{aligned} \quad (14)$$

which of course becomes identical to (6) when $\tilde{m}^2 \rightarrow m_e^2$. As in the free electron case, the antineutrino result may be obtained from (14) by interchanging $s \leftrightarrow u$.

For clarity, we first consider the ionization of a Hydrogen atom being initially in its ground state. The energy spectrum of the ionized electron is obtained by averaging over the bound electron momenta according to its wave function (see Eqs.(15) of [5]), and subsequently changing the $d\sigma/du$ -distribution to $d\sigma/dE_4$, which brings in the derivative du/dE_4 . We thus get

$$\frac{d\sigma_{\text{H}}^{\nu e}}{dE_4} = \frac{1}{64\pi E_1 E_2} \int \frac{d\phi_2 d\cos\theta_2}{(2\pi)^3(s - \tilde{m}^2)} \frac{p_2^2 dp_2}{|\tilde{\Psi}_{100}(p_2)|^2 |F|^2} \left| \frac{du}{dE_4} \right| . \quad (15)$$

The variables (p_2, θ_2, ϕ_2) are the momentum and angles of the bound electron in the rest frame of the atom, (compare (A.1)); and⁴ $\tilde{\Psi}_{100}(p_2)$ is the ground state momentum wave function in momentum space defined in (A.16) of Appendix A.2. Finally E_2 is determined through (10), which for the H ground state ($n = 1, l = 0$) is given by

$$\epsilon = \epsilon_{1s}^H = -\frac{m_e \alpha^2}{2} = -13.6 \text{eV} . \quad (16)$$

The kinematics are fully explained in Appendix A.1; (compare (4)). According to it, for any (θ_2, ϕ_2) in the range (A.3), and any value of the bound electron's momentum p_2 and the incoming neutrino energy E_1 , the polar angle of the ionization electron θ_4 is a function of its energy E_4 given by⁵ (A.6). This function is used to determine through (A.9), the expression for du/dE_4 needed in (15)

²See Appendix A.2.

³Justified because we neglect any spin dependence on the wave function.

⁴This wave function has no angular dependence, because of the vanishing of the orbital angular momentum.

⁵See the discussion immediately after (A.6) for resolving any ambiguity.

We also note that the angular dependence of the integrant in (15) is only due to (A.9) and the effect of (A.4) on $|F|^2$. The angular integration is done numerically, with its range fixed by (A.3). For the numerical evaluation of the p_2 -integral, the relevant part of the p_2 -range is determined by the form of the electron wave function, as discussed immediately after (A.16) and at the end of Appendix A.2.

We next turn to the general case of any of the noble gas atoms He, Ne, Ar, Kr and Xe. Their wave functions are discussed in Appendix A.2 [8]. Since for noble atoms all electronic shells are complete, a summation of the form

$$\sum_{m=-l}^l |Y_{lm}|^2 = \frac{2l+1}{4\pi} ,$$

always appears in the wave function contribution to ionization, washing out any angular dependence induced by it. As a result, the energy distribution of the ionization electron for any noble atom, normalized to one electron per unit volume, may be obtained from (15) by replacing

$$\begin{aligned} |\tilde{\Psi}_{100}(p_2)|^2 \rightarrow \frac{1}{Z \cdot 4\pi} \left\{ & 2[\tilde{R}_{10}(p_2)]^2 + 2[\tilde{R}_{20}(p_2)]^2 + 6[\tilde{R}_{21}(p_2)]^2 \right. \\ & + 2[\tilde{R}_{30}(p_2)]^2 + 6[\tilde{R}_{31}(p_2)]^2 \\ & + 10[\tilde{R}_{32}(p_2)]^2 + 2[\tilde{R}_{40}(p_2)]^2 + 6[\tilde{R}_{41}(p_2)]^2 \\ & \left. + 10[\tilde{R}_{42}(p_2)]^2 + 2[\tilde{R}_{50}(p_2)]^2 + 6[\tilde{R}_{51}(p_2)]^2 \right\} , \end{aligned} \quad (17)$$

where $\tilde{R}_{nl}(p_2)$ are the radial momentum wave functions defined in (A.13), and Z is the atomic number.

Focusing now to within the curly brackets in the r.h.s of (17), we remark that by restricting to just the first (one, three, five, eight, all) terms, we obtain respectively the results for the (He, Ne, Ar, Kr, Xe) atoms, provided the appropriate Z value is used. The corresponding atomic wave functions are discussed in Appendix A.2 and [8].

3 Neutrino ionization of Atoms.

Using (15, 16) and the H-wave function in (A.16), we obtain the results in Fig.3 describing the energy distributions of the knocked out electron in $\nu_e(\bar{\nu}_e)$ ionization of Hydrogen, normalized to one electron per unit volume. The results for various incoming neutrino energies are shown. The corresponding distributions for He, Ne and Xe atoms are shown in Figs.4, 5 and 6 respectively, using the wave functions of Appendix A.2 and the parameters tabulated in [8]. For the electron binding energies in the various atoms and electronic states, we use the experimental values [9]

$$\text{He : } \epsilon_{1s}^{He} = -24.6eV , \quad (18)$$

$$\text{Ne : } \epsilon_{1s}^{Ne} = -870.2\text{eV} , \epsilon_{2s}^{Ne} = -48.5\text{eV} , \epsilon_{2p}^{Ne} = -21.7\text{eV} \quad (19)$$

$$\begin{aligned} \text{Xe : } \epsilon_{1s}^{Xe} &= -34561\text{eV} , \epsilon_{2s}^{Xe} = -5453\text{eV} , \epsilon_{2p}^{Xe} = -4893\text{eV} , \\ \epsilon_{3s}^{Xe} &= -1149\text{eV} , \epsilon_{3p}^{Xe} = -961\text{eV} , \epsilon_{3d}^{Xe} = -681.4\text{eV} , \\ \epsilon_{4s}^{Xe} &= -213.2\text{eV} , \epsilon_{4p}^{Xe} = -145.7\text{eV} , \epsilon_{4d}^{Xe} = -68.3\text{eV} , \\ \epsilon_{5s}^{Xe} &= -23.3\text{eV} , \epsilon_{5p}^{Xe} = -12.5\text{eV} . \end{aligned} \quad (20)$$

As seen from Figs.2-6 the energy distribution in all $\nu_e(\bar{\nu}_e)$ -induced cross sections is maximal at small $E_e = E_4$.

Concerning Figs.3,4, 5, 6 we may also remark that for E_1 in the few 10keV range, the differential $d\sigma/dE_4$ ionization cross sections per electron are always at the level of $10^{-50}\text{cm}^2\text{eV}^{-1}$. Moreover, they are always smaller than the "free electron" ones, approaching them from bellow as E_1 increases; see the (c) and (d) parts of each of these figures. For a fixed E_1 -value though, $d\sigma/dE_4$ decreases as we go from Hydrogen to Xenon.

The integrated $\nu_e(\bar{\nu}_e)$ -ionization cross sections for final electron energies $E_4 > m_e + 10\text{eV}$, are shown in Fig.7. Here again the cross sections are normalized to one electron per unit volume. In the same figure the corresponding integrated cross section off free electrons are also included. As seen from Fig.7a,b, both these cross sections are of the order of 10^{-47}cm^2 at $E_1 \sim 15\text{keV}$, increasing with the neutrino energy. The ratio of the ionization cross section to the free electron one is shown in Fig.7c,d. It is evident that the ionization cross section is always smaller than the free one, approaching it from below. For H and He the approach is very fast, but it becomes much slower for heavier atoms; see *e.g.* the results for Ne and Xe. Thus at $E_1 \sim 50\text{keV}$ the Ne cross section is still about 5% smaller than the free e-one, while for Xe the decrease is at the $\sim 30\%$ level.

Such integrated ionization cross sections for H, He and Ne have already appeared in [5]. The present results are consistent with those. We should point out though that in [5], the integrated cross sections were calculated over the entire physical region $E_4 > m_e$. Moreover, in that work we had used a very rough approximation for the He wave function based on the Z_{eff} -idea, while the Ne results were based on the old fit of Tubis [10]. Thus although the present results are consistent with those of [5], prospective users should rely more on the present ones based on [8]. After all, it is only here that the energy distribution of the ionization electron appears.

The Xenon case is particularly interesting. Although the "per electron" cross section for a few keV neutrinos might be almost half of the Hydrogen one, the fact that there exist 54 electrons in each Xe atom actually induces a gain.

We have already estimated that for ν_e or $\bar{\nu}_e$ in the 10 keV level, the oscillation length is about 150 meters; see (1). Consequently, the other neutrino flavors should also be generated in an experiment where the initial ν_e or $\bar{\nu}_e$ scatters on a volume filed with a noble gas. Thus *e.g.* in Tritium decay experiment, $\bar{\nu}_\mu$ and $\bar{\nu}_\tau$ should also appear in relative amounts determined by the mixing angles and the distance from the source.

The treatment of the ν_μ effects is exactly the same as for ν_e , the only difference being that in (6, 14) we now have to use the second set of the neutrino vector and axial

couplings listed in (3); compare (2). The resulting differential cross for scattering off a free electron is then given Fig.8, which is strikingly different from the corresponding $\nu_e(\bar{\nu}_e)$ result shown in Fig.2. Thus, at the 10 keV range, the $\nu_e(\bar{\nu}_e)$ cross section off a free electron, is more than a factor of 3 larger than the corresponding ν_μ or ν_τ cross sections. A similar situation arises also in Xe ionization; compare the ν_μ induced ionization shown in Fig.9, to the corresponding ν_e effect in Fig.6. Moreover, the E_e distributions tend to have a local minimum at low final electron energies in Figs.8,9, in contrast to the local maximum if Figs.2-6.

It is worth remarking also on the basis of Figs.8 and 9, that the ν_μ and $\bar{\nu}_\mu$ results are almost identical. This is due to the fact that $\tilde{v}_e \simeq 0$ (compare (3)), which makes the squared amplitudes in (6, 14) almost $s \leftrightarrow u$ symmetric. The ν_τ results are of course identical to those for ν_μ ; compare (2).

We next briefly address the problem of the flavor oscillation of the neutrino inducing the noble gas ionization. Since for reasonable gas-densities the vacuum oscillation treatment should be adequate, the oscillation probabilities may be written as

$$P(\nu_e \rightarrow \nu_\mu + \nu_\tau) = \sin^2(2\theta_{12}) \cos^4(\theta_{13}) \sin^2\left(\frac{\Delta_{12}L}{4E_1}\right) + \sin^2(2\theta_{13}) \sin^2\left(\frac{\Delta_{13}L}{4E_1}\right), \quad (21)$$

$$P(\nu_e \rightarrow \nu_e) = 1 - P(\nu_e \rightarrow \nu_\mu + \nu_\tau), \quad (22)$$

assuming three active and no sterile neutrinos. Here θ_{12} , θ_{23} , θ_{13} are the 3 mixing angles, while $\Delta_{ij} \equiv m_j^2 - m_i^2$ denote the mass differences between the neutrino masses satisfying $|\Delta_{13}| \simeq |\Delta_{23}| \gg |\Delta_{12}|$ [1, 4], and L is the distance from the source. We note that there is no dependence on the neutrino CP-violating phase δ in (21, 22), and that these same formulae describe antineutrino oscillations also.

Thus, as an initially produced ν_e transverses *e.g.* a Xe target, the ionization cross section per electron varies with L as

$$\frac{d\sigma_{\text{Xe}}}{dE_4} = [1 - P(\nu_e \rightarrow \nu_\mu + \nu_\tau)] \cdot \frac{d\sigma_{\text{Xe}}^{\nu e}}{dE_4} \Big|_{\nu=\nu_e} + P(\nu_e \rightarrow \nu_\mu + \nu_\tau) \cdot \frac{d\sigma_{\text{Xe}}^{\nu e}}{dE_4} \Big|_{\nu=\nu_\mu}, \quad (23)$$

in the r.h.s of which (15, 17) should be used for $\nu = \nu_e$ and $\nu = \nu_\mu$ respectively. Correspondingly for antineutrinos.

Using the experimental Δ_{ij} values, we find that the oscillation length of the first term of $P(\nu_e \rightarrow \nu_\mu + \nu_\tau)$ (see (21)) is about 150m for an incoming neutrino energy of $E_1 \simeq 10\text{keV}$, while the oscillation length of the second term is only about 5.6m. Since θ_{13} is known to be very small, the picture created by (23) will then consist of a few hundred meter oscillation, modulated by a much weaker one of a few meter size [4]. The strength of the modulation is determined by θ_{13} .

Depending, therefore, on the achievable experimental accuracy, the study $\bar{\nu}_e$ oscillations in Tritium decay may help further constraining the neutrino mixing angles and masses. This would be most interesting for θ_{13} , for which information might be derived if a future experiment manages to be sensitive to both oscillation lengths governing (21).

4 Conclusions

In this paper we have presented the formalism for the ionization of atoms by bombarding them with neutrinos of any flavor in the keV energy range. The interest in this energy range originates from the fact that the oscillations lengthes for neutrinos in the few keV range become rather small, allowing the possibility of studying the oscillations observed in the solar neutrino and KAMLAND experiments, by means of a terrestrial experiment of small size. Neutrinos in this energy may be obtained from various possible beta decays; most notably Tritium decay producing antineutrinos.

Motivated by this, we have undertaken the present extensive study of the ionization of atoms by neutrinos. To this purpose, we have developed a method for treating the bound state effects for Hydrogen as well as the noble gases He, Ne, Ar, Kr and Xe. In our method, the energy of the bound electron in each atomic state is fixed by its binding energy, while its momentum varies according to the distribution determined by the momentum wave function, thereby generally forcing the electron to get off-shell. For simplicity, we have neglected spin effects in the atomic wave functions, which in turn allows to average the elementary νe -cross section over all initial and final spin states. In our calculations we have used the most recent spin independent non-relativistic wave function results of 1993 listed in [8]. It should be straightforward to extend this method to any other atom.

These results should be very accurate. If required by future experiments they could be further improved by including radiative corrections to the elementary amplitude, and also including spin and relativistic effects to the atomic wave functions. The later certainly necessitates the collaboration with atomic physics experts.

Extensive applications have been presented for H, He, Ne and Xe. We have found that at the 10 keV neutrino energy range, the differential cross sections $d\sigma/dE_e$ are at the $10^{-50} cm^2/eV$ level for $\nu_e(\bar{\nu}_e)$ -induced precesses, while the integrated cross section is of the order of $10^{-47} cm^2$.

At the 10–20 keV neutrino energy range, atomic effects are very important and cannot be ignored. Particularly for Xe, the binding of the electrons inside the atom is so strong, that it reduces the per-electron cross section by almost a factor of two, compared to the neutrino scattering off free electrons. Nevertheless, the existence of 54 electrons in each Xe-atom, would make it the most interesting target for oscillations studies.

Of course, as the incoming neutrino energy increases beyond *e.g.* the 100 keV region, all these "per-electron" ionization cross sections approach the neutrino cross section off free electrons, always from below.

We have also compared the ν_e induced reactions, with those induced by ν_μ or ν_τ ; the later two being equal to each other. The difference between the two comes from the fact that ν_e reactions involve both charged and neutral current diagrams, while for ν_μ , ν_τ only neutral currents contribute. As a result, the energy distribution of the final electron in the ν_μ reactions tends to have a local minimum at low electron energies, in contrast to the local maximum expected for the corresponding ν_e effect. Moreover for 10keV neutrinos, the magnitude of the ν_e integrated cross section should be larger than the ν_μ one by more than a factor 3.

As an overall conclusion we may state that if such small cross sections become measurable one day, neutrino atomic ionization experiments may be used to test the electroweak theory at keV energies by looking for oscillations, or anomalous interactions. One interesting observation in this respect is the possibility to obtain information on the third mixing angle θ_{13} , for which only an upper bound exists at present. To fully achieve this though, it may be necessary to augment the present ionization study with an analogous one concerning neutrino atomic excitations to higher discreet states, where the observable signature would of course be the observation of the emitted photons.

Acknowledgement

The support of the “Bundesministerium für Bildung, Wissenschaft, Forschung und Technologie”, Bonn under contract 05HT1PEA9, and the support by European Union under the RTN contracts HPRN-CT-2000-00148 and HPRN-CT-2000-00152, are gratefully acknowledged. P.I.P. is also grateful to the Institut für Physik, Universität Dortmund, for the hospitality extended to him during part of this work.

Appendix A.1 Kinematics

In the rest frame of the atom, defining the \hat{z} -axis along the direction of the incoming neutrino, and the xz -plane as the plane where the (final) ionization electron lies, we write, (compare eq. (4))

$$P_1^\mu = \begin{pmatrix} E_1 \\ 0 \\ 0 \\ E_1 \end{pmatrix}, \quad P_2^\mu = \begin{pmatrix} E_2 \\ p_2 \sin \theta_2 \cos \phi_2 \\ p_2 \sin \theta_2 \sin \phi_2 \\ p_2 \cos \theta_2 \end{pmatrix}, \quad P_4^\mu = \begin{pmatrix} E_4 \\ p_4 \sin \theta_4 \\ 0 \\ E_4 \cos \theta_4 \end{pmatrix}, \quad (\text{A.1})$$

where E_1 is the energy of the initial neutrino; $(E_2, p_2, \theta_2, \phi_2)$ are the energy, momentum and angles of the electron bound inside the atom; and (E_4, p_4, θ_4) are the energy, momentum and polar angle of the freely moving final ionization electron. By definition, the range of these angles is

$$0 < \theta_4 < \pi, \quad (\text{A.2})$$

$$0 < \theta_2 < \pi, \quad 0 < \phi_2 < 2\pi. \quad (\text{A.3})$$

The standard variables defined in (5) become

$$\begin{aligned} s &= \tilde{m}^2 + 2E_1(E_2 - p_2 \cos \theta_2), \\ t &= m_e^2 - 2E_1(E_4 - p_4 \cos \theta_4), \\ u &= 2E_1(E_4 - p_4 \cos \theta_4 - E_2 + p_2 \cos \theta_2). \end{aligned} \quad (\text{A.4})$$

where the definition (12) is used, and (13) is of course satisfied.

The requirement of

$$P_3^2 = (P_1 + P_2 - P_4)^2 = 0 \quad (\text{A.5})$$

implied by the negligibly small mass of the neutrino, leads to an equation determining $\cos \theta_4$ in terms of E_4 and E_1 . In the free electron case, this is linear in $\cos \theta_4$, and it can be solved immediately leading to eq. (7).

For bound electrons, however, (A.5) leads to a quadratic equation in $\cos \theta_4$, which also depends on the momentum and spherical angles of the bound electron. It is then important to discriminate between the two mathematically possible solutions, among which only one is physically acceptable. To do this we first note that the general solution of (A.5), may be written as

$$\tan\left(\frac{\theta_4}{2}\right) = \frac{\zeta_1 \pm \sqrt{\zeta_1^2 - \zeta_2}}{2\zeta_3}, \quad (\text{A.6})$$

where

$$\begin{aligned} \zeta_1 &= 2p_4 p_2 \sin \theta_2 \cos \phi_2, \\ \zeta_2 &= 4\left\{[E_4(E_1 + E_2) - \xi]^2 - p_4^2(E_1 + p_2 \cos \theta_2)^2\right\}, \\ \zeta_3 &= E_4(E_1 + E_2) - \xi + p_4(E_1 + p_2 \cos \theta_2), \end{aligned} \quad (\text{A.7})$$

$$\xi = -E_1 p_2 \cos \theta_2 + E_1 E_2 + \frac{m_e^2 + \tilde{m}^2}{2} . \quad (\text{A.8})$$

A detail study indicates that whenever both θ_4 solutions of (A.6) satisfy (A.2), the physically acceptable one is given by the upper (lower) sign of (A.6), depending on whether⁶ $\zeta_1 > 0$ ($\zeta_1 < 0$) respectively. The criterion for selecting one solution requires θ_4 to be a continuous function of the variables collecting in the integrations.

Once the physically acceptable solution in (A.6)) has been identified, du/dE_4 entering (15) is determined from

$$\begin{aligned} \frac{du}{dE_4} &= -2E_1 \left(1 - \frac{E_4}{p_4} \cos \theta_4 + p_4 \frac{d\theta_4}{dE_4} \sin \theta_4 \right) , \\ \frac{d\theta_4}{dE_4} &= \frac{E_4 [E_1 \cos \theta_4 + p_2 (\cos \theta_2 \cos \theta_4 + \sin \theta_2 \sin \theta_4 \cos \phi_2)] - (E_1 + E_2)p_4}{p_4^2 [E_1 \sin \theta_4 + p_2 (\cos \theta_2 \sin \theta_4 - \sin \theta_2 \cos \theta_4 \cos \phi_2)]} . \end{aligned} \quad (\text{A.9})$$

Finally, the requirement $\zeta_1^2 \geq \zeta_2$ (note the square root in (A.6)) imply that the range over which E_4 can vary in an ionization is

$$E_4^{(2)} \leq E_4 \leq E_4^{(1)} , \quad (\text{A.10})$$

with

$$\begin{aligned} E_4^{(1,2)} &= \frac{\xi(E_1 + E_2) \pm \xi_1 \sqrt{\xi^2 - m_e^2 [(E_1 + E_2)^2 - \xi_1^2]}}{(E_1 + E_2)^2 - \xi_1^2} , \\ \xi_1 &= \sqrt{(E_1 + p_2 \cos \theta_2)^2 + p_2^2 \sin^2 \theta_2 \cos^2 \phi_2} . \end{aligned} \quad (\text{A.11})$$

Appendix A.2 The Atomic Wave Functions

In (15) and the corresponding formulae for the heavier atoms, we need the atomic wave functions in the momentum space, with all spin effects neglected. These are related to the coordinate wave functions by

$$\tilde{\Psi}_{nlm}(\vec{k}) = \int d^3r \Psi_{nlm}(\vec{r}) e^{-i\vec{k}\cdot\vec{r}} , \quad (\text{A.12})$$

where nlm denote the usual quantum numbers characterizing atomic states. The radial momentum wave function defined by the first function in the r.h.s of⁷

$$\tilde{\Psi}_{nlm}(\vec{k}) = (-i)^l \tilde{R}_{nl}(k) Y_{lm}(\hat{k}) , \quad (\text{A.13})$$

⁶According to the first of (A.7), this is equivalent to $\cos \phi_2$ being positive (negative) respectively.

⁷ $Y_{lm}(\hat{k})$ is the usual spherical harmonic function depending on the momentum angles.

is related to the radial wave function in coordinate space through

$$\tilde{R}_{nl}(k) = 4\pi \int_0^\infty dr r^2 R_{nl}(r) j_l(kr) , \quad (\text{A.14})$$

where $j_l(kr)$ is a spherical Bessel function. The normalization is such that

$$\int \frac{d^3k}{(2\pi)^3} |\tilde{\Psi}_{nlm}(\vec{k})|^2 = 4\pi \int_0^\infty \frac{k^2 dk}{(2\pi)^3} |\tilde{R}_{nl}(k)|^2 = 1 . \quad (\text{A.15})$$

We next turn to the explicit form of momentum wave functions for the ground state of the various atoms. For Hydrogen, the standard ground state wave function is

$$\tilde{\Psi}_{100}(k) = \frac{1}{\sqrt{4\pi}} \tilde{R}_{10}(k) = \frac{8\sqrt{\pi}(Z_H)^{5/2}}{(k^2 + (Z_H)^2)^2} , \quad (\text{A.16})$$

with $Z_H = m_e\alpha$ being the inverse Bohr radius of the H-atom. In all cases involving integrals over the Hydrogen momentum wave function, we integrated over the range $0 \leq k \lesssim 3Z_H$, which describes very accurately the relevant momentum of the bound electron.

For the heavier atoms we follow [8] based on the Roothann-Hartree-Fock (RHF) approach, also explained in [11]. Accordingly, the radial momentum wave functions are written as

$$\tilde{R}_{nl}(k) = \sum_j C_{jln} \tilde{S}_{jl}(k) , \quad (\text{A.17})$$

in terms of the RHF functions $\tilde{S}_{jl}(k)$ in momentum space, related to $S_{jl}(r)$ given in ref. [8] through

$$\tilde{S}_{jl}(k) = 4\pi \int_0^\infty dr r^2 S_{jl}(r) j_l(kr) , \quad (\text{A.18})$$

in analogy to (A.14). Since $S_{jl}(r)$ also depend on a parameter called n_{jl} and tabulated in [8], the corresponding momentum RHF functions are:

$$\begin{aligned} l &= 0 \\ n_{j0} = 1 &\rightarrow \tilde{S}_{j0}(k) = \frac{16\pi Z_{j0}^{5/2}}{(Z_{j0}^2 + k^2)^2} , \\ n_{j0} = 2 &\rightarrow \tilde{S}_{j0}(k) = \frac{16\pi Z_{j0}^{5/2}(3Z_{j0}^2 - k^2)}{\sqrt{3}(Z_{j0}^2 + k^2)^3} , \\ n_{j0} = 3 &\rightarrow \tilde{S}_{j0}(k) = \frac{64\sqrt{10}\pi Z_{j0}^{9/2}(Z_{j0}^2 - k^2)}{5(Z_{j0}^2 + k^2)^4} , \end{aligned}$$

$$\begin{aligned}
n_{j0} = 4 &\rightarrow \tilde{S}_{j0}(k) = \frac{64\pi Z_{j0}^{9/2}(5Z_{j0}^4 - 10Z_{j0}^2k^2 + k^4)}{\sqrt{35}(Z_{j0}^2 + k^2)^5} , \\
n_{j0} = 5 &\rightarrow \tilde{S}_{j0}(k) = \frac{128\sqrt{14}\pi Z_{j0}^{13/2}(3Z_{j0}^4 - 10Z_{j0}^2k^2 + 3k^4)}{21(Z_{j0}^2 + k^2)^6} ,
\end{aligned} \tag{A.19}$$

$$l = 1$$

$$\begin{aligned}
n_{j1} = 2 &\rightarrow \tilde{S}_{j1}(k) = \frac{64\pi k Z_{j1}^{7/2}}{\sqrt{3}(Z_{j1}^2 + k^2)^3} , \\
n_{j1} = 3 &\rightarrow \tilde{S}_{j1}(k) = \frac{64\sqrt{10}\pi k Z_{j1}^{7/2}(5Z_{j1}^2 - k^2)}{15(Z_{j1}^2 + k^2)^4} , \\
n_{j1} = 4 &\rightarrow \tilde{S}_{j1}(k) = \frac{128\pi k Z_{j1}^{11/2}(5Z_{j1}^2 - 3k^2)}{\sqrt{35}(Z_{j1}^2 + k^2)^5} , \\
n_{j1} = 5 &\rightarrow \tilde{S}_{j1}(k) = \frac{128\sqrt{14}\pi k Z_{j1}^{11/2}(35Z_{j1}^4 - 42Z_{j1}^2k^2 + 3k^4)}{105(Z_{j1}^2 + k^2)^6} ,
\end{aligned} \tag{A.20}$$

$$l = 2$$

$$\begin{aligned}
n_{j2} = 3 &\rightarrow \tilde{S}_{j2}(k) = \frac{128\sqrt{10}\pi k^2 Z_{j2}^{9/2}}{5(Z_{j2}^2 + k^2)^4} , \\
n_{j2} = 4 &\rightarrow \tilde{S}_{j2}(k) = \frac{128\pi k^2 Z_{j2}^{9/2}(7Z_{j2}^2 - k^2)}{\sqrt{35}(Z_{j2}^2 + k^2)^5} .
\end{aligned} \tag{A.21}$$

The parameters $(C_{jln}, n_{jl}, Z_{jl})$ appearing in (A.17, A.19-A.21) are all given in the Tables in [8]. Parameters (C_{jln}, n_{jl}) are dimensionless, while Z_{jl} are expressed in units of $m_e\alpha = 3.73$ keV in [8].

We also note that, according to (A.19-A.21, A.17) and [8], the highest Z_{j0} for each atomic state determines the relevant range where the bound electron's momentum lies⁸. In most cases, this range is found to be $0 \leq k \lesssim 3 \max(Z_{j0})m_e\alpha$.

⁸Compare (A.16) and the related variable Z_H .

References

- [1] H. S. Gurr, F. Reines and H. W. Sobel, Phys. Rev. Lett. **28**:1406 (1972); M. Apollonio *et al.* (CHOOZ collaboration), Phys. Lett. **B446**:415 (1999); Y. Fukuda et al. (Superkamiokande Collaboration), Phys. Rev. Lett. **82**:2644 (1999); A. Ianni (for the Borexino Collaboration), Nucl. Phys. **A663**:791 (2000); J.N. Bahcall, M.C. Gonzalez-Garcia, C. Peña-Garay, hep-ph/0406294.
- [2] J. Bouchez and I. Giomataris, CEA/Saclay internal note, DAPNIA/01-07, Jun 2001; Y. Giomataris, Ph. Rebougeard, I.P. Robert and G. Charpak, Nucl. Instr. Meth. **A376**:29 (1996); J.L. Collar, I. Giomataris, "Low-background applications of Micromegas detector technology", presented at IMAGING 2000 conference, Stockholm, 28/06/2000-01/07/2000, DAPNIA/00-06.
- [3] T. Araki *et al.* (KamLAND Collaboration), hep-ex/0405035.
- [4] For a recent review see *e.g.* M. Maltoni, T. Schwetz, M.A. Tortola and J.W.F. Valle, hep-ph/0405172; G. Sigl, hep-ph/04008165, and references therein.
- [5] G.J. Gounaris, E.A. Paschos, and P.I. Porfyriadis, Phys. Lett. **B525**:63 (2002).
- [6] Y.V. Gabonov, Y.L. Dobrynnin and V.I. Tikhonov, Sov. J. Nucl. Phys. **22**:170 (1976).
- [7] S.A. Fayans, V.Y. Dobretsov, A.B. Dobrosvetov, Phys. Lett. **B20**:1 (1992); V.Y. Dobretsov, A.B. Dobrosvetov, S.A. Fayans, Sov. J. Nucl. Phys. **55**:1180 (1992).
- [8] C. F. Bunge, J. A. Barrientos, and A. V. Bunge, Atomic Data and Nuclear Data Tables **53**:113 (1993); C. F. Bunge, J. A. Barrientos, and A. V. Bunge and J.A. Cogordan Phys. Rev. **A46**:3691 (1992).
- [9] The electron binding energies for the various atoms are taken from <http://www.webelements.com/webelements/>.
- [10] A. Tubis, Phys. Rev. **102**:1049 (1956); C. Zener, Phys. Rev. **36**:51 (1930); P.M. Morse, L.A. Young and E.S. Haurwitz, Phys. Rev. **48**:948 (1935).
- [11] J.C. Slater in "Quantum Theory of Atomic Structure", vol I, Mc. Graw-Hill Book Company, N.Y., 1960.

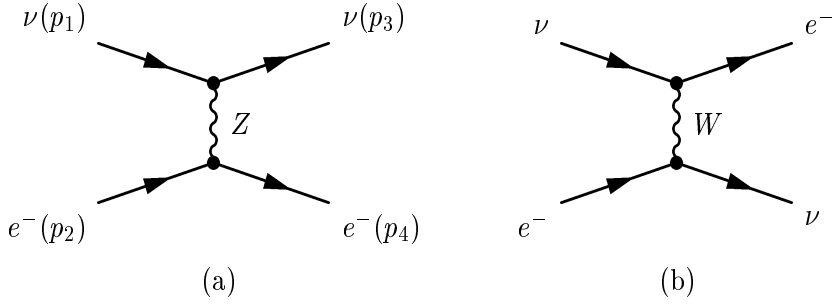


Figure 1: The Feynman diagrams for $\nu_e e^-$ -scattering.

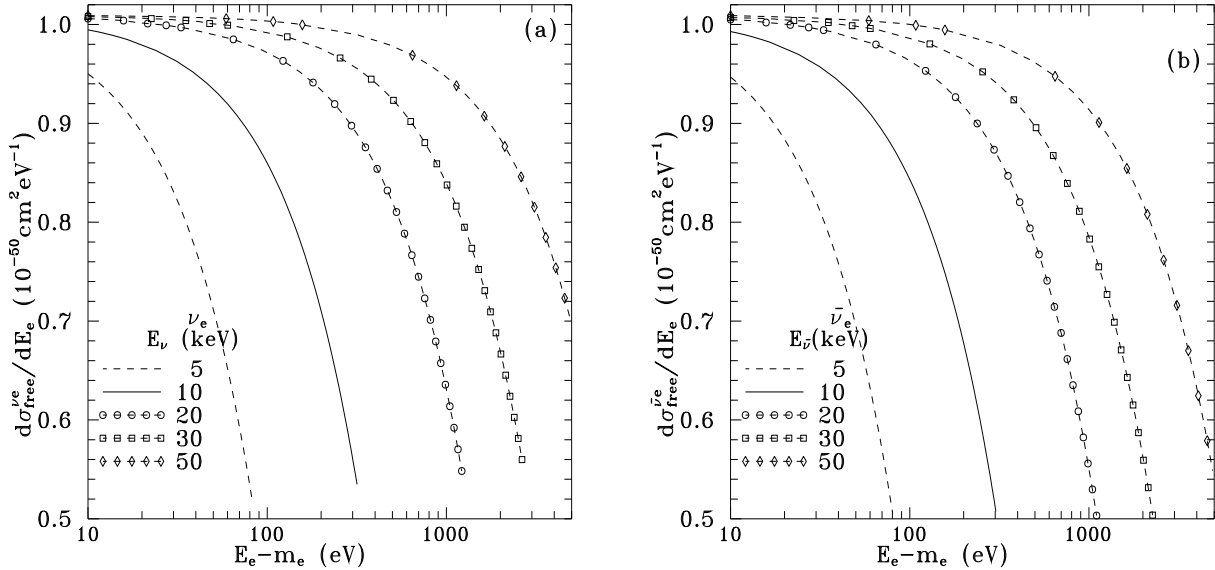


Figure 2: The energy distribution of the final electron in $\nu_e e^-$ (a) or $\bar{\nu}_e e^-$ (b) scattering, at the rest frame of a free initial e^- . Here $E_e \equiv E_4$ is the final electron energy, and E_ν ($E_{\bar{\nu}}$) denote the incoming neutrino (antineutrino) energy E_1 ; see text.

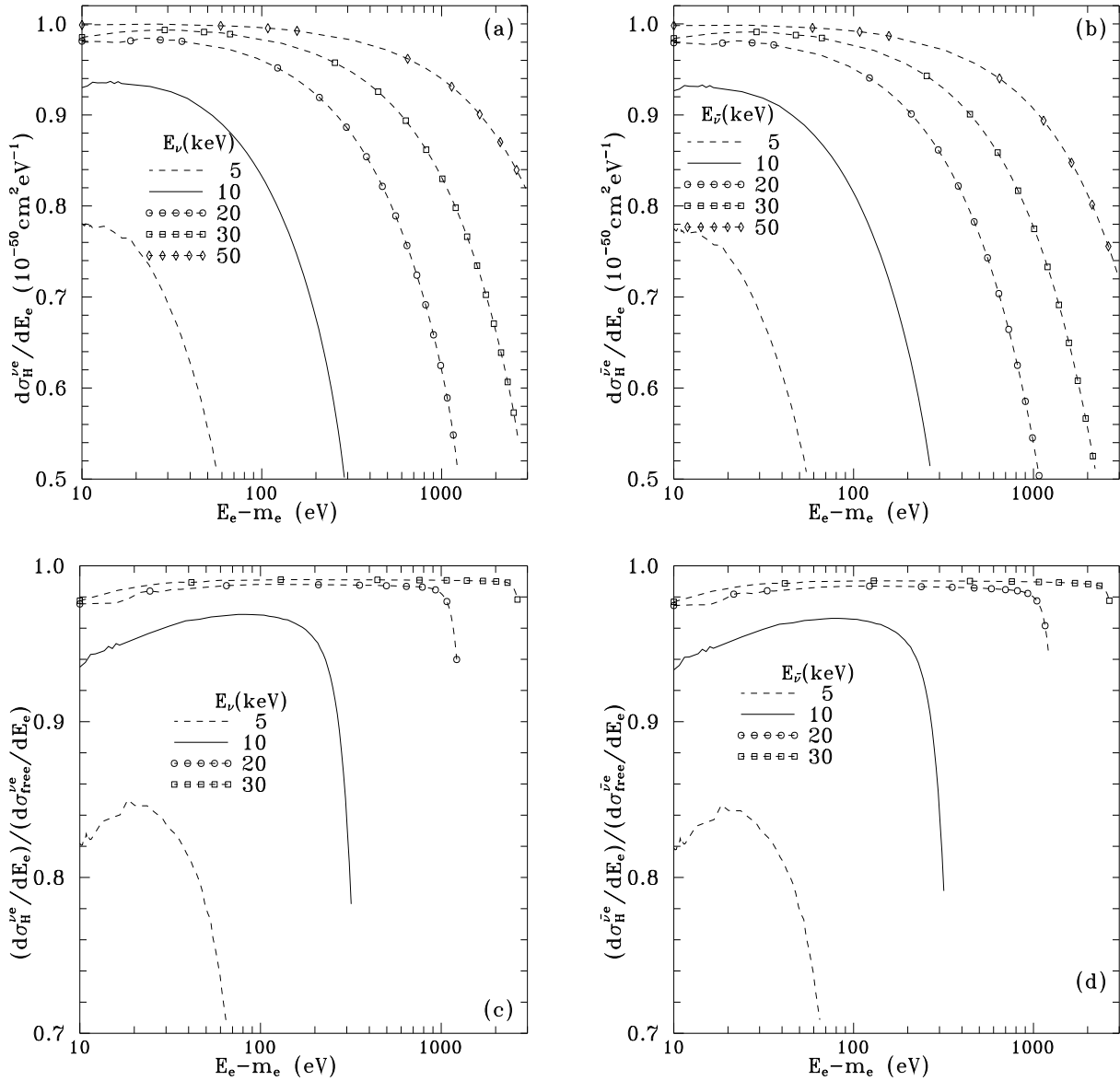


Figure 3: The electron energy distribution in ν_e (a) or $\bar{\nu}_e$ (b) ionization of H , and their respective ratio (c) and (d) to the corresponding distributions when the initial electron is assumed as free. Variables defined as in caption of Fig.2.

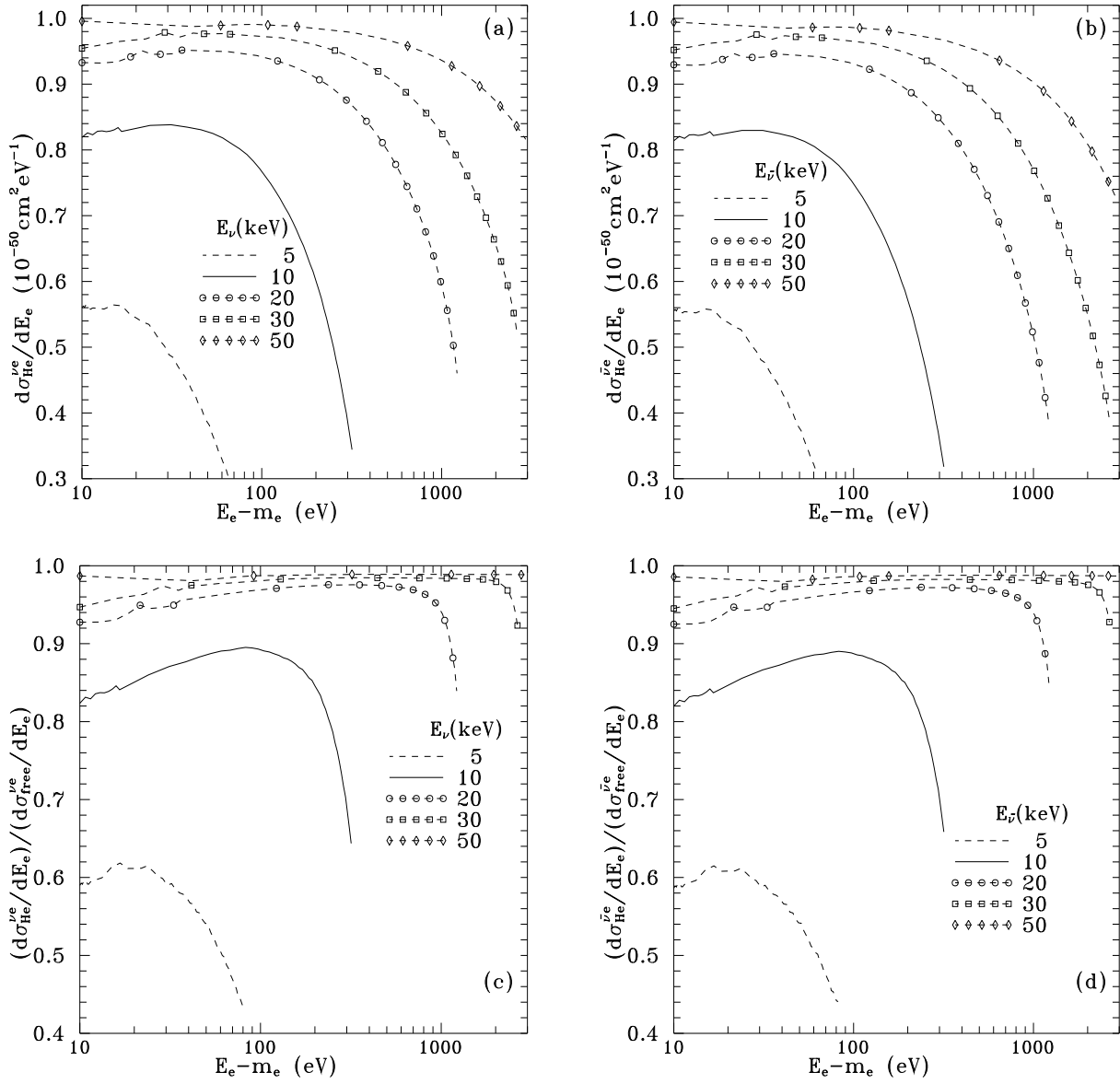


Figure 4: The electron energy distribution in ν_e (a) or $\bar{\nu}_e$ (b) ionization of He normalized to one e^- per unit volume, and their respective ratio (c) and (d) to the corresponding distributions when the initial electron is assumed as free; see Fig.2. Variables defined as in caption of Fig.2.

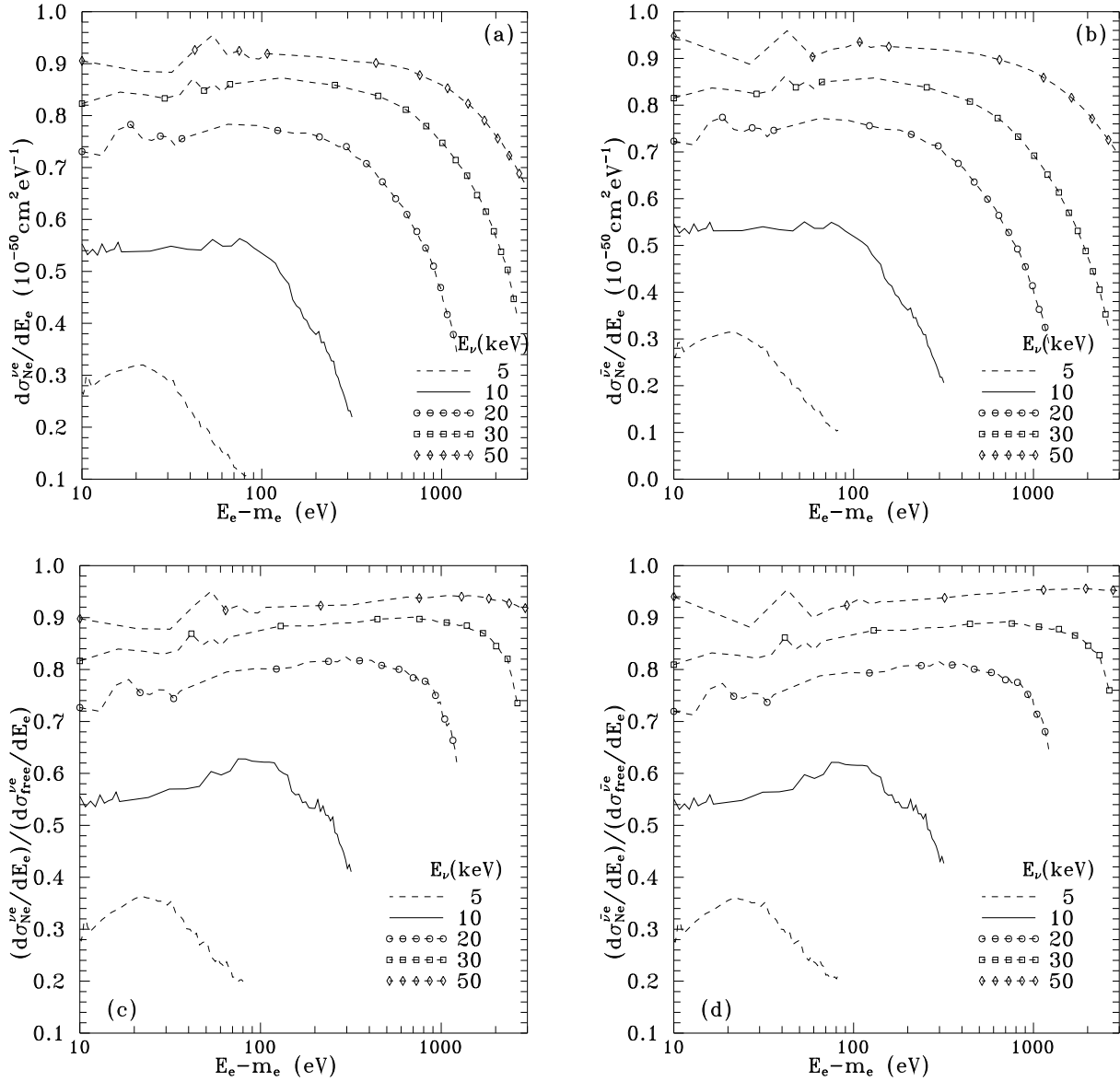


Figure 5: The electron energy distribution in ν_e (a) or $\bar{\nu}_e$ (b) ionization of Ne normalized to one e^- per unit volume, and their respective ratio (c) and (d) to the corresponding distributions when the initial electron is assumed as free; see Fig.2. Variables defined as in caption of Fig.2.

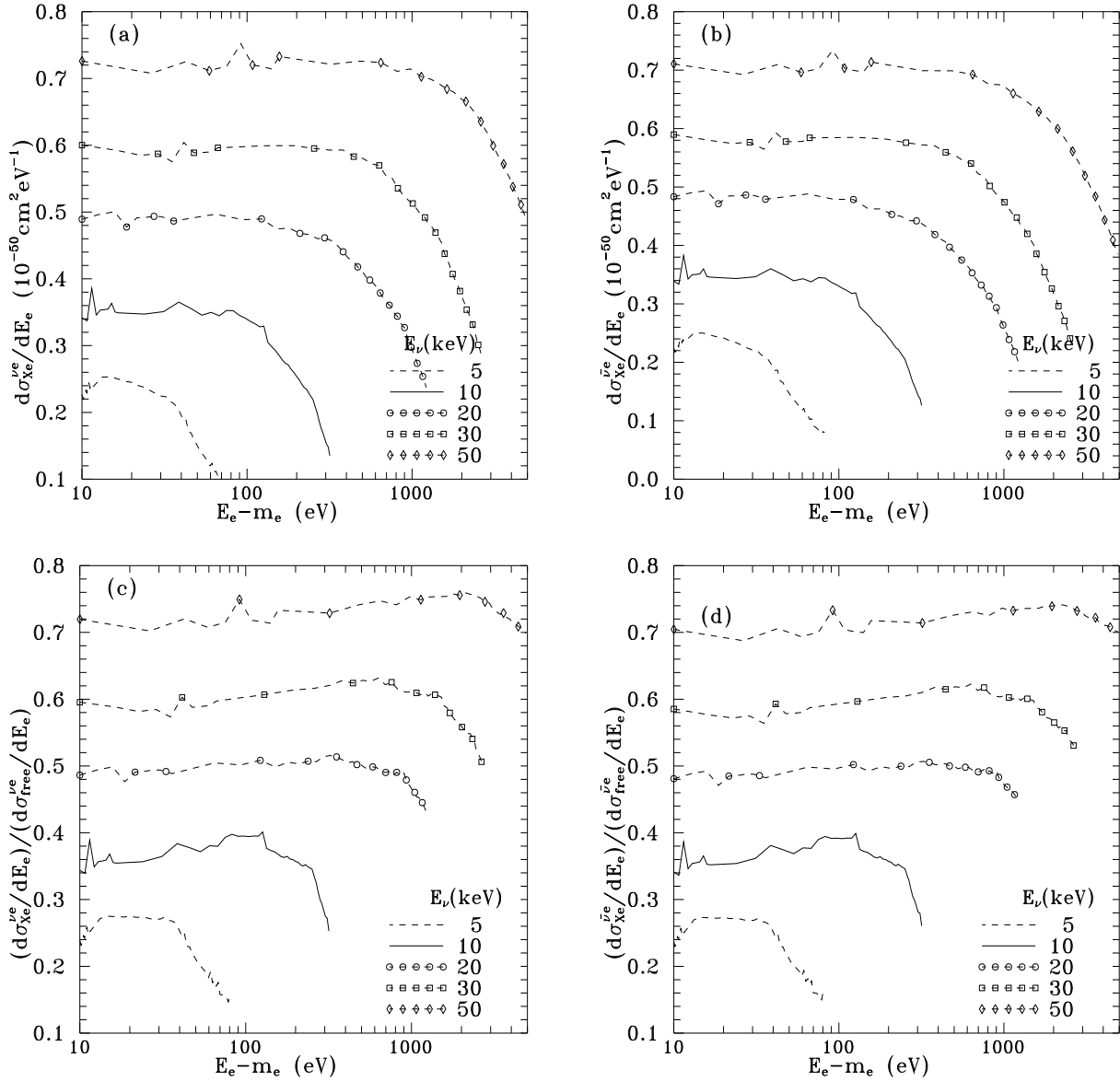


Figure 6: The electron energy distribution in ν_e (a) or $\bar{\nu}_e$ (b) ionization of Xe normalized to one e^- per unit volume, and their respective ratio (c) and (d) to the corresponding distributions when the initial electron is assumed as free; see Fig.2. Variables defined as in caption of Fig.2.

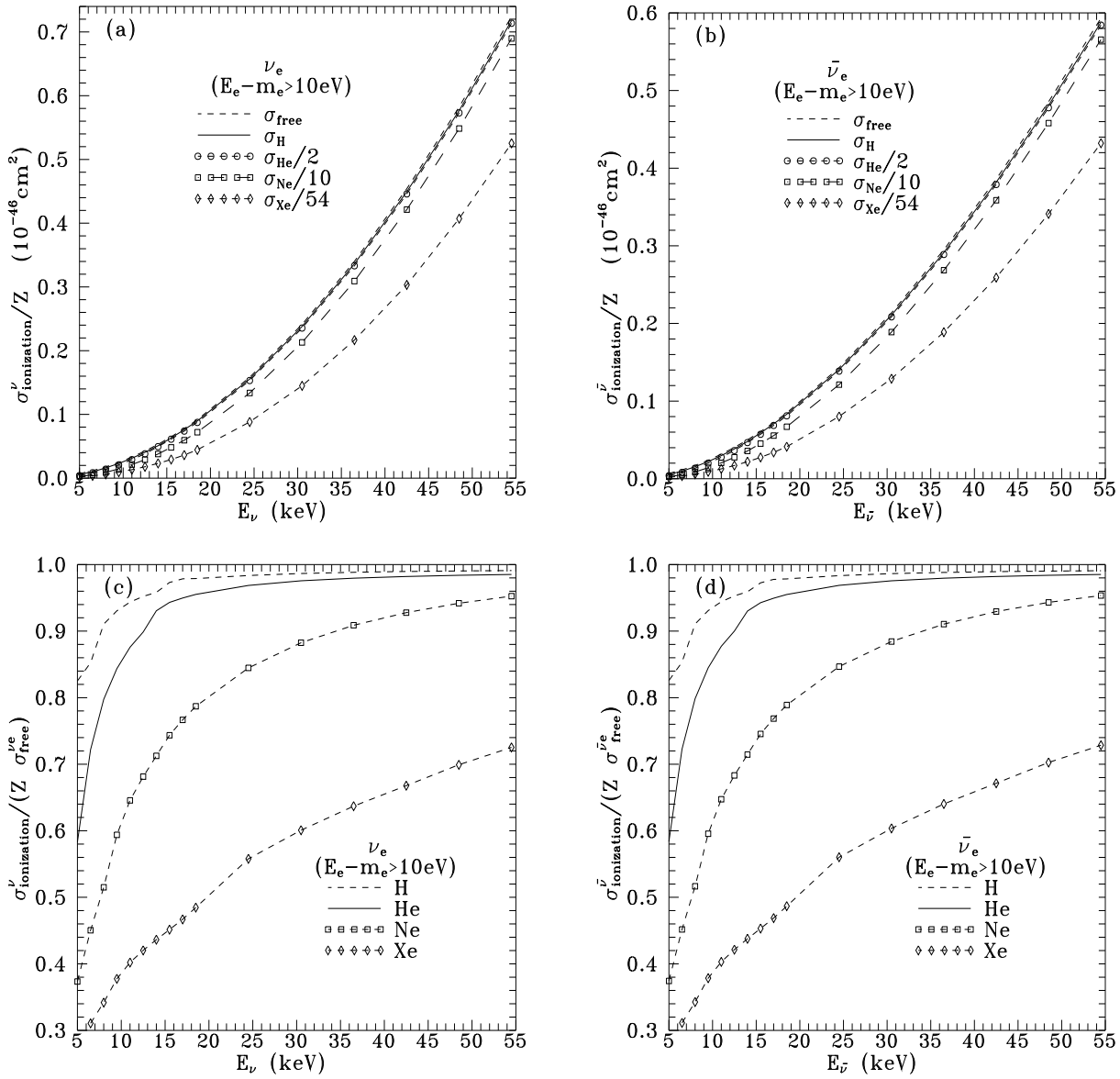


Figure 7: The ν_e (a) [$\bar{\nu}_e$ (b)] ionization integrated cross sections for H, He, Ne and Xe atoms divided by Z , and the cross section off free electrons at rest, as a function of the ν_e [$\bar{\nu}_e$] energy. The ratios of these ionization cross section, to the free electron ones are given in (c) and (d) respectively.

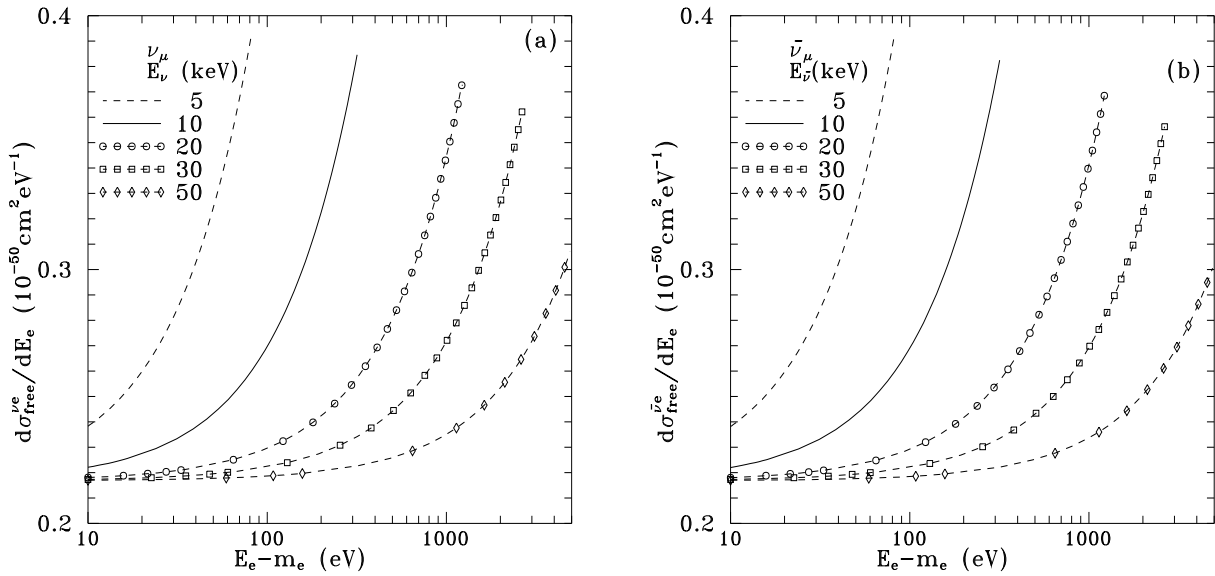


Figure 8: The energy distribution of the final electron in $\nu_\mu e^-$ (a) or $\bar{\nu}_\mu e^-$ (b) scattering, at the rest frame of a free initial e^- . Here $E_e \equiv E_4$ is the final electron energy, and E_ν ($E_{\bar{\nu}}$) denote the incoming neutrino (antineutrino) energy E_1 . Identical results for ν_τ .

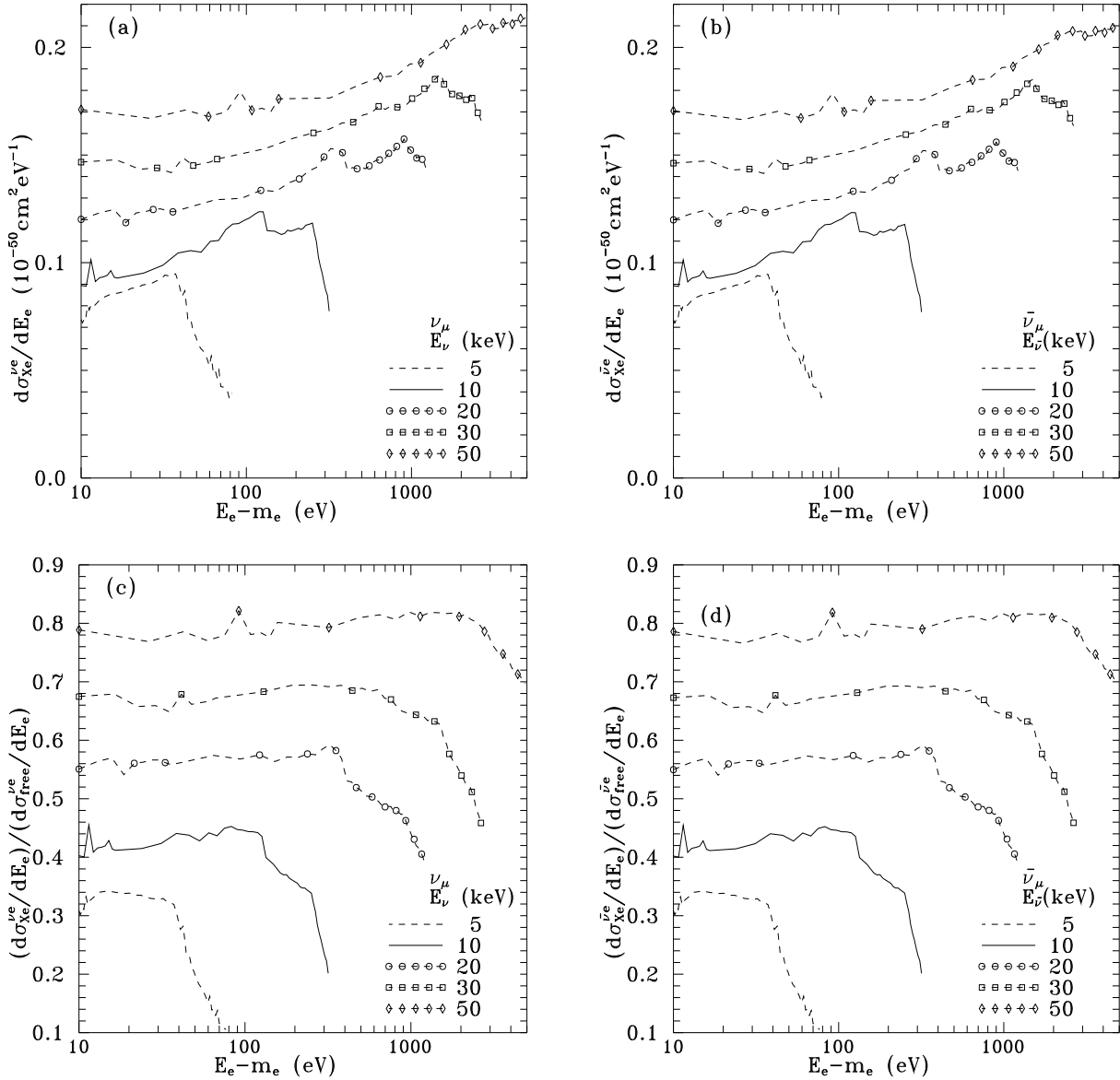


Figure 9: The electron energy distribution in ν_μ (a) or $\bar{\nu}_\mu$ (b) ionization of Xe normalized to one e^- per unit volume, and their respective ratio (c) and (d) to the corresponding distributions when the initial electron is assumed as free; see Fig.8. Identical results for ν_τ